Journal of Materials Chemistry B

PAPER

View Article Online
View Journal | View Issue

Published on 19 September 2016. Downloaded by Synchrotron Radiation Library on 11/09/2017 07:25:19.

Cite this: J. Mater. Chem. B, 2016, 4, 6694

Preparation and characterization of a biodegradable polyurethane hydrogel and the hybrid gel with soy protein for 3D cell-laden bioprinting†

Hsin-Hua Lin,[a] Fu-Yu Hsieh,[a] Ching-Shiow Tseng[b] and Shan-hui Hsu*[acd]

Received 17th June 2016,
Accepted 16th September 2016

DOI: 10.1039/c6tb01501h

www.rsc.org/MaterialsB

3D printing shows great potential for fabricating customized scaffolds for tissue regeneration. Using hydrogel as a bioink for cell printing provides a biological platform for basic research and potential medical treatments. In this study, a waterborne poly(ε-caprolactone) (PCL)-based biodegradable polyurethane (PU) with a soft segment replaced with 20 mol% of poly(L-lactide) (PLLA) diol or poly(D,L-lactide) (PDLLA) diol was prepared. These two PUs formed compact packing structures at temperatures ≥37 °C. They responded differently to temperature changes and the presence of electrolytes because of the difference in the free volume. With their thermal-responsive properties, both PU dispersions could form a gel in 3 min with the gel modulus reaching about 6–8 kPa after 30 min. To enhance the structural integrity during layer-by-layer deposition, the hybrid hydrogel of PU and soy protein isolate (PU/SPI hybrid) was further developed. The PU/SPI hybrid dispersion could undergo rapid gelation at 37 °C with the modulus reaching 130 Pa in 1 min. Moreover, the PU/SPI hybrid gel was readily blended with cells and printed at 37 °C without preheating. Neural stem cells (NSCs) were embedded in the hydrogels and analyzed for cell viability, metabolism, proliferation, and gene expression of neural-related markers. Cells cultured in the PU/SPI hybrid construct had better survival and proliferation than those in the PU gel. The PU/SPI hybrid ink may provide unique rheological properties for direct cell/tissue printing at 37 °C and a biomimetic microenvironment for cell survival, growth, and differentiation.

1. Introduction

A large proportion of patients around the world suffer from disorders of the central nervous system (CNS) including severe traumatic injuries or neurodegenerative diseases such as strokes, Alzheimer's disease, and Parkinson's disease.[1,2] There are a lack of effective treatments so far. Neural stem cells (NSCs) have shown great promise as a transplantation therapy in the last decades because they have the capacity for regeneration and can be differentiated into different types of functional cells under specific surroundings.[3–5] The formation and maintenance of a functional neural network requires an appropriate support.[6] A proper biomimetic 3D scaffold provides physical support for NSCs and an environment for cell/tissue crosstalk, leading to the establishment of a functional nervous system. Recent advances in 3D printing technology enables the production of functional 3D scaffolds combining biomaterials, cells, and bioactive components.[7,8] Recognizing the need for creating a permissive environment for nerve regeneration, a promising bioink used for 3D bioprinting is important for neural tissue engineering. A hydrogel is a type of material with a high water capacity and is commonly used in the field of extrusion-based bioprinting.[9] Researchers have presented a variety of studies on bioprintable hydrogels (*i.e.*, alginate, gelatin, and collagen).[10–13] However, there are still limitations in these biomaterials. Some of the existing biomaterials lack proper mechanical properties, even though they can be manipulated by chemical modification and crosslinking or by altering the molecular weight and concentration.[14–16] Increasing the polymer concentration of a hydrogel often enhances the mechanical properties of the hydrogel, and printed constructs with a better integrity can be obtained. However, the higher polymer concentration also leads to greater viscoelasticity and larger pressure and shear stress for extrusion of the hydrogel, which may harm the embedded cells.[6]

[a] Institute of Polymer Science and Engineering, National Taiwan University, No. 1, Sec.4 Roosevelt Road, Taipei 10617, Taiwan, Republic of China. E-mail: shhsu@ntu.edu.tw; Fax: +886-2-3366-5237; Tel: +886-2-3366-5313
[b] Department of Mechanical Engineering, National Central University, Taoyuan, Taiwan, Republic of China
[c] Research and Development Center for Medical Devices, National Taiwan University, Taipei, Taiwan, Republic of China
[d] Institute of Cellular and System Medicine, National Health Research Institutes, Zhunan, Taiwan, Republic of China

† Electronic supplementary information (ESI) available. See DOI: 10.1039/c6tb01501h

This journal is © The Royal Society of Chemistry 2016

Published on 19 September 2016. Downloaded by Synchrotron Radiation Library on 11/09/2017 07:25:19.

Therefore, the rheological properties, structural integrity, and biocompatibility of hydrogels need to be improved and optimized for printing.

Biodegradable polyurethane (PU) is used in many biomedical applications because of its advantageous mechanical properties, flexibility, and biocompatibility.[17,18] PU consisting of PCL and PEG oligomer segments was used as a scaffolding material for repairing neural and venous defects.[19] By fine-tuning the chemistry and ratio of the mixed oligodiols in PU, a biodegradable PU can be synthesized as an aqueous dispersion that may undergo a sol to gel transition when the temperature of the dispersion is raised to 37 °C.[20] With such sol–gel transition behavior at room temperature, cells may be encapsulated into a thermo-responsive PU dispersion as a cell-laden bioink for printing at 37 °C.[21] However, because of the relatively long curing time, the bioink must be preheated before printing. The time frame where printing can be performed (working window) is rather narrow.

To improve the printability of the synthesized polymer and further enhance the cell affinity, a plant-derived polymer, soy protein isolate (SPI), was introduced to the PU dispersion to prepare the hybrid bioprinting ink. Soy protein has a thermoplastic nature as well as an inherent biocompatibility, which was demonstrated both *in vitro*[22,23] and *in vivo*.[24] Because of its flexibility, soy protein materials can also be successfully fabricated into scaffolds by a 3D printer.[25] Hydrogen bonds, disulfide bonds, and hydrophobic interactions of soy proteins can assist in the formation of 2-D and 3-D stable structures.[22,23] We hypothesized that the unique intramolecular and intermolecular forces of SPI and the possible interaction with PU may facilitate the solidification process of the hybrid hydrogel and maintain the structure during 3D printing.

In this study, a thermo-sensitive waterborne biodegradable PU dispersion was prepared using a mixed diol (L-lactide diol/D,L-lactide diol and PCL diol) as the soft segment. The rheological properties of PU dispersed in the electrolyte-containing medium were investigated. We observed that the PU dispersion could be blended with cells, preheated, and subsequently printed and deposited, but only a few layers. The hybrid hydrogel of PU with SPI was further developed to enhance the rheological properties, cell viability, printability, and structural integrity. We demonstrated that the PU/SPI hybrid could be mixed with cells and printed at 37 °C layer-by-layer. Therefore, the PU/SPI hybrid hydrogel is a potential bioink formula for direct 3D cell printing.

2. Materials and methods

2.1. Synthesis of waterborne biodegradable PU

The soft segment in the PUs consisted of PCL diol (M_n 2000 Da, Sigma-Aldrich) or PCL diol with another oligodiol, poly(L-lactide) (PLLA) diol or poly(D,L-lactide) (PDLLA) diol (M_n ~ 2000 Da). The latter two diols were synthesized from a ring-opening polymerization of dilactide. The 1,3-propandiol (1,3-PDO, Alfa Aesar), a ring-opening agent, with 0.05% of catalyst T-9 was used to open the ring structure of L-lactide (Purac) and D,L-lactide (Purac) at 145 °C for 8 h, which were further purified by absolute ethanol.

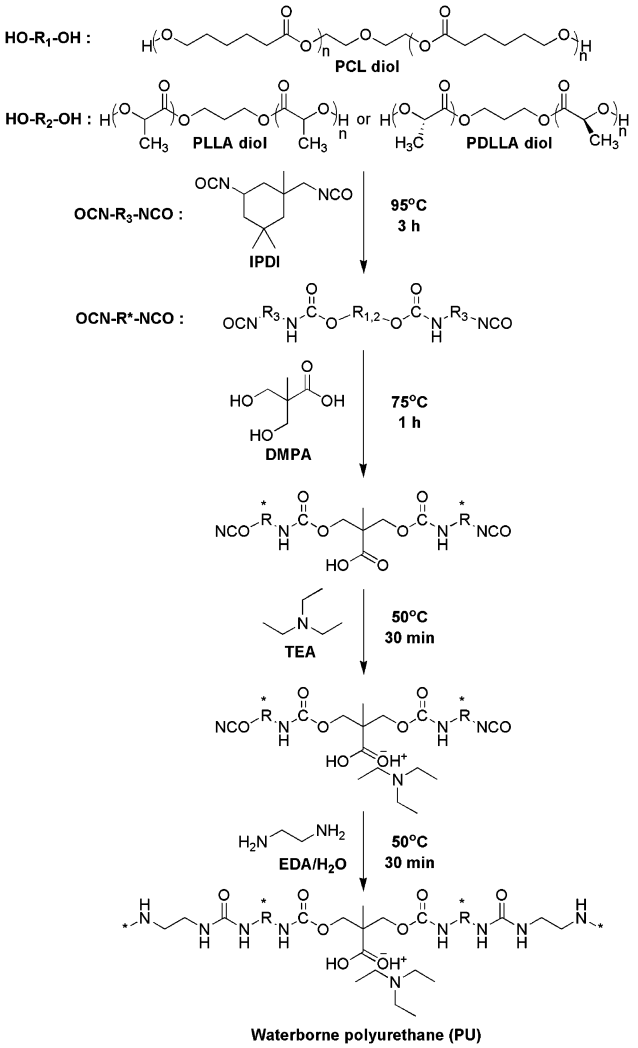

Fig. 1 Synthesis scheme for waterborne biodegradable PU (PCL100, PCL80LL20, and PCL80DL20).

The molecular weight of the oligodiol was confirmed by the end-group analysis using nuclear magnetic resonance (NMR).

Biodegradable PU was synthesized from an eco-friendly process previously developed.[26] Three different PU dispersions were prepared in this study, as illustrated in Fig. 1. PU containing 100% of the PCL oligodiol in the soft segment was abbreviated as PCL100, and PU containing 80% of the oligodiol and 20% of the PLLA (or PDLLA) oligodiol in the soft segment was abbreviated as PCL80LL20 (or PCL80DL20). To mix the PCL diol and other oligodiol, the two oligodiols were firstly added into a four-necked vessel and mechanically stirred under a nitrogen environment at 95 °C for 30 min. After the two oligodiols fused and mixed homogeneously, isophorone diisocyanate (IPDI, Evonik Degussa, GmbH) and tin(II) 2-ethylhexanoate (T-9, Alfa Aesar) catalyst were added to carry out the prepolymerization under nitrogen for 3 h (180 rpm). Afterwards, 2,2-bis(hydroxymethyl) propionic acid (DMPA, Sigma-Aldrich) and 0.27% methyl ethyl ketone (MEK, J. T. Baker) were sequentially added to the reactor under reflux at 75 °C for 1 h. The temperature was then cooled

Published on 19 September 2016. Downloaded by Synchrotron Radiation Library on 11/09/2017 07:25:19.

down to 50 °C. The carboxylic groups of DMPA were neutralized by triethylamine (TEA, RDH) for 30 min. Eventually, ethylenediamine (EDA, Tedia) diluted with deionized water was poured into the reactor under vigorous stirring for water dispersion. The stoichiometric ratio of IPDI/oligodiols/DMPA/EDA/TEA was 3.52 : 1 : 1 : 1.52 : 1.[26] After removal of the residual solvent and neutralizing agent by vacuum distillation, the final water dispersion of PU was obtained. The solid content was about 30% and could be adjusted or added to with culture media or electrolytes. The molecular weight of PU was determined by dissolving the PU films in dimethylacetamide (DMAc) using a JASCO gel permeation chromatography (GPC) system equipped with an RI detector (RI-930).

2.2. Size and zeta potential of the nanoparticle dispersion

The PU dispersion for the experiments was diluted with distilled deionized water to a concentration of 3000 ppm. The electrolyte-dependent properties of the PU dispersion were investigated in the presence of additional salts. The electrolyte was sodium chloride (0.9% NaCl) or the culture medium [low glucose Dulbecco's Modified Eagle's Medium (LG-DMEM, Gibco) and sodium bicarbonate (Sigma-Aldrich)]. The concentration of the medium in the PU dispersion was adjusted to the same concentration as that for the cell culture. The hydrodynamic radius (R_h) of the PU dispersion was measured by DLS (Nanosizer, Delsa™ Nano Beckman Counter), and the zeta potential was determined on the basis of electrophoretic light scattering measurements.

2.3. Characterization by small-angle X-ray light scattering (SAXS)

SAXS measurements were carried out at the beamline 23A at the National Synchrotron Radiation Research Center (NSRRC) in Hsinchu, Taiwan. The intensity of the X-ray was operated at 10 keV. Samples were loaded into a 2.5 mm thick holder and measured in a scattering vector (q-range) of 0.0025 to 0.1 $Å^{-1}$. The PU dispersions with a concentration of 1500 ppm were investigated at 25 °C and 37 °C, and the PU dispersions (30 wt%) were examined at 60 °C. The SAXS profiles were further analysed by the Schulz distribution fitting model.[27] The consistent slope in the low-q region could be described as the fractal dimension of the packing structure.

2.4. Rheological measurements of the thermally-induced sol–gel transition

The dynamic rheological properties of the dispersions (with or without electrolytes) were measured by a rheometer (Rheometric RS-5, TA instrument) with cone and plate geometry. The diameter of the cone was 40 mm, and the angle was 2°. The concentration of the PU dispersions (with and without electrolytes) was 30%. For additional electrolytes in the PU dispersions, the concentration of $NaCl_{(aq)}$ was 0.9% and the concentration of the medium in the PU dispersion was exactly the same as that for the cell culture. Hybrid gel dispersions were prepared from the stock PCL80DL20 30% and SPI 19% solutions. SPI (PRO-FAM® 974) was directly purchased from the Archer Daniels Midland Company (ADM, USA). The hydrogel composed of PU and SPI was sterilized by exposure to UV for 30 min before use. The SPI solution was firstly prepared by dissolving SPI in a phosphate buffered saline (PBS) solution warmed at 70 °C for 30 min. Different weight ratios between PCL80DL20 and SPI were employed for rheological measurements. To keep the samples from drying during the measurement period of time, an environmental regulation chamber was equipped to maintain the ambient humidity. The 0.8 ml sample was then injected on the plate and retained at 37 °C. The shear storage and loss modulus were immediately recorded at a frequency of 1 Hz and an oscillatory strain of 1%.

2.5. Characterizations by X-ray diffraction (XRD) and attenuated total reflectance Fourier transform infrared spectroscopy (ATR-FTIR)

The crystalline structure of PU (solid) was determined using an X-ray diffractometer (XRD, Bede D1, UK). The data were obtained with a CuKα radiation (λ = 1.54 Å) source and scanned over a range of 2θ = 5° to 30°.

PU films were scanned using a FTIR spectrophotometer (Spectrum 100 model, Perkin Elmer) with an ATR mode setup. The PU films were immersed into LG-DMEM (without fetal bovine serum, FBS, Gibco) for 24 h and dried with a freeze dryer. Spectra were obtained under a resolution of 1 cm^{-1} with the wavenumber in the range of 650 to 4000 cm^{-1}. The proportion of the hydrogen bound carbonyl groups of the total carbonyl groups in the structure was calculated from the relative absorbance at 1670 cm^{-1} and 1730 cm^{-1}.

2.6. Calcium adsorption by atomic absorption (AA) analysis

PU films cast on covered glasses were placed into a 24-well plate, and 1 ml of the culture medium was loaded into each well. After 24 h of immersion, the medium was collected to measure the calcium concentration in the solution by atomic absorption (AA) spectrometry (iCE 3300; Thermo Scientific, USA). The stock culture medium was used as the control group. The amount of calcium adsorbed by each PU film was determined based on the difference between the calcium concentration in the solution before and after PU immersion.

2.7. Cell culture and bioprinting

L929 fibroblasts (mouse skin fibroblast cells, Bioresource Collection and Research Center, Taiwan) and murine neural stem cells (NSCs) were used in this study. L929 cells were cultured in LG-DMEM with 3.7 g L^{-1} sodium bicarbonate, 10% FBS, and 1% penicillin streptomycin amphotericin (PSA, Caisson) at 37 °C in a 5% CO_2 incubator. NSCs were obtained as previously described[19] and were cultured in HG-DMEM and Ham's F-12 (DMEM/F12) supplemented with 10% FBS, 400 μg ml^{-1} G418 (Invitrogen), and 1% penicillin–streptomycin (PS, Caisson) and maintained in the 5% CO_2 incubator. Cells (density 1 × 10^7 cells per ml) were then labelled with a red fluorescent dye (2 × 10^{-6} M, PKH26 Red Fluorescence Cell Linker Kit, Sigma-Aldrich) for observation in hydrogels.

Three different bioinks were prepared: pure PCL80LL20 and PCL80DL20 hydrogels and a PCL80DL20/SPI hybrid gel.

 This journal is © The Royal Society of Chemistry 2016

Published on 19 September 2016. Downloaded by Synchrotron Radiation Library on 11/09/2017 07:25:19.

Pure cell-laden PU inks were created by the following procedures. A 30% PU dispersion with the culture medium was heated at 60 °C to form the hydrogel precursor. After the PU dispersion became a hydrogel, fibroblasts were embedded in the PU gel at a density 2×10^6 cells per ml at room temperature. For the hybrid gel, according to previous rheological analysis, the PCL80DL20 and SPI dispersion were mixed homogeneously in a 1.3 : 1 weight ratio at 25 °C. The cells were directly encapsulated in the hybrid gel at a density of 2×10^6 cells per ml.

The cell-containing dispersion was loaded into a sterilized syringe with a 337 μm size, and the structure was fabricated using a commercial 3D bioprinter (Regenovo, China), which was placed in a laminar cabinet. The mixture was extruded under a pressure ranging from 50 to 60 kPa on the 37 °C platform, which led to solidification and stabilization of the printed hydrogels. The cell-laden hydrogel constructs were added with the culture medium and placed in the incubator immediately after printing. The culture medium was refreshed every other day.

2.8. Cell viability and proliferation

The cell viability in the distinct hydrogels was evaluated by the Nucleocounter® NC-3000™, which is an image cytometer that uses fluorescence imaging to characterize cell properties. The cells were stained in Solution 5, which contained propidium iodide (PI) and acridine orange, to mark the dead cells and serve as a counterstain, respectively, and a fluorophore VB-48 that bound to glutathione to analyze the cell health. The number of live (healthy)/live (unhealthy)/dead cells in the hydrogel were counted based on the staining. Because of the limitations of transmittancy, the cells in the PCL80DL20/SPI hybrid hydrogel could not be precisely measured.

Cell proliferation in the scaffolds after 0, 24, and 48 h of culture time was evaluated by the MTT assay described below. At each time point, the culture medium was removed, and the constructs were washed with PBS. The tetrazolium dye [3-(4,5-dimethylthiazol-2-yl)-2,5-diphenyltetrazolium bromide (MTT) 200 μl, 1 mg ml^{-1}, Sigma-Aldrich] was added and incubated at 37 °C for 8 h. After that, the purple formazan was solubilized with absolute ethanol and determined by the optical density (O.D.) at 570 nm using a multifunctional microplate reader (SpectraMax® M5, USA). The cell viability (percentage) was expressed as the measured O.D. value normalized to the initial value (at 0 h).

After a 48 h culture, the samples were firstly washed in PBS water in order to conduct the immunohistochemical staining. The anti-Ki67 antibody (1 : 100; GeneTex) and secondary antibody (1 : 500; GeneTex) were used to assess the cell proliferation.

2.9. Cell metabolism

Cell metabolism in the various hydrogels was measured by a Seahorse XFp analyzer (Seahorse Bioscience, USA), and the protocol was based on the manufacturer's instruction. Briefly, the cells mixed with distinct hydrogels were seeded into the microchamber for culturing overnight before the measurement. The cellular oxygen consumption rate (OCR) was measured to assess the mitochondrial respiration activity of the NSCs encapsulated in different hydrogels.

2.10. Gene expression analysis for cells printed with hydrogels

The total RNA was isolated from the NSC-laden hydrogels using the Trizol® reagent (Invitrogen, USA) after 3 days. The RNA was converted into cDNA by utilizing the RevertAid™ First Strand cDNA Synthesis Kit (MBI Fermentas St. Leon-Rot, Germany). A real-time polymerase chain reaction (qRT-PCR) was performed using the DyNAmo Flash SYBR Green qPCR Kit (Finnzymes Oy, Espoo, Finnland) and conducted by a Chrome 4 PTC-200 Thermal Cycler (MJ Research, USA) under the denaturing program at 95 °C for 10 min, followed by 30 cycles of denaturing at 95 °C for 30 s, annealing at 55 °C for 30 s, and extension at 72 °C for 45 s. The gene expression was normalized to the housekeeping gene, glyceraldehyde 3-phosphate dehydrogenase (GAPDH).

2.11. Statistical analysis

All quantitative values were reported as mean ± standard deviation with multiple samples. Reproducibility was confirmed in three independent experiments. Statistical analysis was performed with the Student's *t*-tests. Differences in the *p*-values of less than 0.05 were considered to be statistically significant and are denoted with asterisks.

3. Results

3.1. Synthesis and characteristics of waterborne PUs

The chemical structures of three PUs (PCL100, PCL80LL20, and PCL80DL20) are illustrated in Fig. 1. All the PU dispersions had a zeta potential below −54 eV, indicating the stability of these nanoparticles in aqueous solutions. The average molecular weight of PCL80LL20 and PCL80DL20 was $\sim 2.6 \times 10^4$ kDa and the weighted average molecular weight was $\sim 4.5 \times 10^4$ kDa.

3.2. Thermo-responsive properties of the PU nanoparticles

The temperature-dependent hydrodynamic radius (R_h) of the PCL80LL20 and PCL80DL20 nanoparticles measured by DLS at 25 °C, 37 °C, and 60 °C is displayed in Table 1 (PCL100 shown in ESI,† Table S1). There was no significant temperature-dependent change in the PCL100 nanoparticles when the

Table 1 Radii of PU nanoparticles at 25 °C, 37 °C, and 60 °C (DLS/SAXS)

	Hydrodynamic radius (R_h, nm)			Radius of Schulz distribution (R_{av}, nm)		
PU NPs	25 °C	37 °C	60 °C	25 °C	37 °C	60 °C
PCL80LL20	18.3 ± 0.3	23.4 ± 0.8	19.7 ± 1.0	17.3 ± 4.0	25.8 ± 7.4	22.3 ± 4.9
PCL80DL20	18.2 ± 0.8	19.9 ± 0.5	21.1 ± 0.7	19.0 ± 3.6	19.0 ± 3.7	27.6 ± 5.9

Published on 19 September 2016. Downloaded by Synchrotron Radiation Library on 11/09/2017 07:25:19.

temperature was 60 °C. The R_h values of the PCL100 nanoparticles were 18.6 nm, 19.3 nm, and 19.1 nm, respectively, at the temperatures of 25 °C, 37 °C, and 60 °C. However, the R_h values of the PCL80DL20 nanoparticles increased from 18.2 to 19.9 nm and the R_h values of the PCL80LL20 nanoparticles increased from 22.3 nm to 23.4 nm when the temperature was raised from 25 °C to 37 °C. At 60 °C, the R_h of PCL80LL20 decreased to 19.7 nm and the R_h of PCL80DL20 increased to 21.1 nm.

Fig. 2(A–C) shows the SAXS profiles of the PU dispersions at 25 °C, 37 °C, and 60 °C. The experimental data for the PCL80DL20 dispersion at 25 °C and 37 °C overlapped with each other (Fig. 2B). The hump position (arrows with a solid line tail) in the SAXS profiles roughly corresponded to the average size of the nanoparticles. When the temperature was elevated to 60 °C, the humps in both PCL80LL20 and PCL80DL20 shifted to the low-q region, revealing the size increases. The average radius (R_{av}) of the PU nanoparticles obtained by the Schulz distribution model is listed in Table 1. No size variation was observed for the PCL80DL20 nanoparticles at 25 °C and 37 °C. In contrast, there was a significant size increase of 8 nm for the PCL80LL20 nanoparticles when the temperature increased from 25 °C to 37 °C. When the temperature was further elevated from 37 °C to 60 °C, the average radius of the PCL80DL20 nanoparticles increased from 19.0 nm to 27.6 nm, and that of the PCL80LL20 nanoparticles decreased from 25.8 nm to 22.3 nm.

As the temperature was elevated to 60 °C, the distance among the PU nanoparticles (both PCL80LL20 and PCL80DL20 nanoparticles) became shorter. The inter-particle distance among the PU nanoparticles at 60 °C was determined from the SAXS profiles (pointed out by arrows with a dash line tail) in Fig. 2A and B. The spacing among the PCL80LL20 nanoparticles was 38.3 nm, while that among the PCL80DL20 nanoparticles was 64.1 nm. The influence of suspending the nanoparticles in the culture medium on the SAXS profiles is shown in Fig. 2C. In the culture medium, the PU nanoparticles formed a network structure. The fractal dimension (D_f) of the PU network in the culture medium was 2.81 for PCL80DL20 and 3.19 for PCL80LL20.

3.3. Electrolyte sensitive behavior of the PU nanoparticles

The R_h value and zeta potential of the PCL80LL20 and PCL80DL20 nanoparticles at 25 °C in water and in the presence of electrolytes are shown in Table 2. In water, the size of both of the nanoparticles was around 18 nm and the zeta potential was about −54 eV. In the presence of electrolytes, the size of the PCL80LL20 nanoparticles changed only slightly (*i.e.*, 17.4 nm in the culture medium and 18.3 nm in an NaCl solution). However, the PCL80DL20 nanoparticles shrank significantly from 18.2 nm to 15.8 nm in the presence of the culture medium with a zeta potential increase from −54.4 eV to −42.5 eV (16.3 nm with −46.6 eV upon the addition of NaCl).

3.4. Rheological properties of the PU dispersions

The rheological changes in the PU dispersions at 37 °C are expressed as storage and loss shear moduli (G' and G'') against time and are shown in the ESI† (Fig. S1). The gelation time and gel modulus (G') after 1, 5, 10, 20, and 30 min are listed in Table 3. The gelation time is the time required for the sol to gel phase transition and is defined by rheology as the point where the storage modulus (G') and loss modulus (G'') intersect with each other. It was observed that the PCL100 dispersion did not

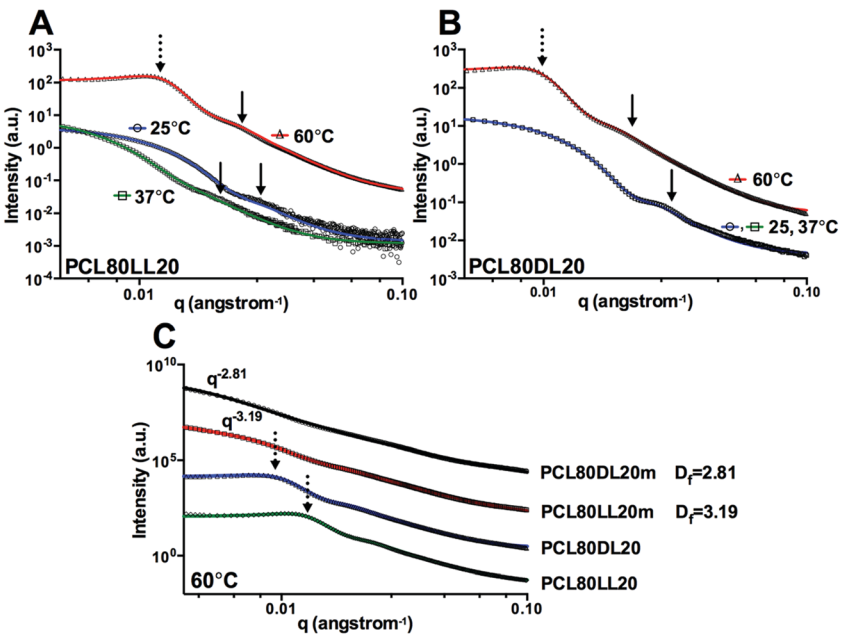

Fig. 2 Profiles of the Schulz distribution model fitting from SAXS measurement for PU dispersions. Black solid arrows correspond to the average size of the nanoparticles. Arrows with dashed lines indicate the inter-particle distance among the PU nanoparticles. (A) PCL80LL20 from 25 °C to 60 °C in water, (B) PCL80DL20 from 25 °C to 60 °C in water, and (C) PCL80LL20 and PCL80DL20 with or without culture medium at 60 °C.

 This journal is © The Royal Society of Chemistry 2016

Published on 19 September 2016. Downloaded by Synchrotron Radiation Library on 11/09/2017 07:25:19.

Table 2 Radii and zeta potentials of PU nanoparticles in pure water and in the presence of electrolytes at 25 °C (DLS)

	In water		In medium		In $NaCl_{(aq)}$	
PU NPs	R_h (nm)	(eV)	R_h (nm)	(eV)	R_h (nm)	(eV)
PCL80LL20	18.3 ± 0.3	−54.8 ± 0.8	17.4 ± 1.0	−54.5 ± 0.3	18.3 ± 0.6	−53.5 ± 1.5
PCL80DL20	18.2 ± 0.8	−54.4 ± 2.0	15.8 ± 1.3	−42.5 ± 1.7	16.3 ± 0.5	−46.6 ± 2.2

Table 3 Rheological properties of aqueous PU dispersions with or without electrolytes at 37 °C

		Gel strength (G', Pa) after				
PUs	Gelation time (s)	1 min	5 min	10 min	20 min	30 min
PCL100 30%	NA	0.4				
PCL80LL20 30%	282	0.1	7.62	1039	4036	6089
PCL80DL20 30%	317	0.6	6.94	893	2358	3792
PCL80LL20 (med) 30%	192	0.13	15.7	1104	4709	7641
PCL80DL20 (med) 30%	187	0.14	53.2	991	3635	6256
PCL80LL20 ($NaCl_{(aq)}$) 30%	120	0.08	370	2215	6160	9435
PCL80DL20 ($NaCl_{(aq)}$) 30%	163	0.46	713	4624	11 098	15 621

undergo a sol–gel transition at 37 °C. On the other hand, the sol–gel transition was found in the PCL80LL20 and PCL80DL20 dispersions at 37 °C when the solid content was either 30% or 25%. The PCL80LL20 30% dispersion in water showed a faster gelation in 282 s compared to the PCL80DL20 30% dispersion (317 s). The gel modulus of the PCL80LL20 (30%) significantly rose from 7.62 Pa at 5 min to 6.1 kPa after 30 min, while that of the PCL80DL20 (30%) was only 3.8 kPa after 30 min.

The rheological changes of the PU dispersion in the culture medium upon the temperature increase to 37 °C are shown in Fig. 3A and B. The rheological properties of the PU dispersions in $NaCl_{(aq)}$ are shown in the ESI† (Fig. S1). It was found that the G' of PCL80DL20 (30% in the culture medium) increased earlier and more steadily than that of PCL80LL20 at 37 °C. The gelation time and G' at various time points are listed in Table 3 and the ESI† (Table S2). The presence of electrolytes had a more obvious effect on the rheological properties of the PCL80DL20 dispersion. In the culture medium, the PCL80DL20 gelled earlier and had a greater G' compared to that in water. The electrolyte effect of NaCl on PCL80DL20 was even more remarkable. In the culture medium, the gelation time of the PCL80LL20 and PCL80DL20 dispersions were similar, ~192 s and 187 s. Moreover, the PCL80DL20 dispersion showed a G' value of 53.2 Pa at 5 min (*vs.* 15.7 Pa for PCL80LL20), which allowed the dispersion to be printed with less collapse. Overall, the rheological behavior of the PCL80DL20 dispersion was more sensitive to electrolytes than that of the PCL80LL20 dispersion.

3.5. Rheological properties of the PCL80DL20/SPI mixed gel

To further increase the time (working window) to print, PCL80DL20 was mixed with SPI in weight ratios of 1 : 1 to 1.7 : 1. The rheological properties of the mixed systems are shown in the ESI† (Fig. S2) and summarized in Table 4. Adding SPI into the PCL80DL20 dispersion dramatically reduced the gelation time. The sol-to-gel transition was too fast to be detected, *i.e.*, before the rheological measurement started. When the mixing ratio was 1.7 : 1 or 1.5 : 1, the initial viscosity was still too low for printing. When the mixing ratio was 1 : 1 or 1.2 : 1, the G' value after 10 min significantly declined to 0.3–0.4 kPa. The optimal mixing ratio of PU/SPI determined by the study was 1.3 : 1, which gave a G' of 0.7 kPa after 10 min and 4.67 kPa after 30 min. The rheological profiles of SPI and PU/SPI in the culture medium are shown in Fig. 3C and D. Again, the culture medium reduced the initial viscosity for printing and increased the gel modulus G' later to create a proper printing time frame. Based on the rheological study, the dispersion of PCL80DL20/SPI at a 1.3 : 1 ratio in the culture medium was selected as the bioink formula for cell printing.

3.6. XRD, ATR-FTIR, and AA spectroscopy

To elucidate the mechanism behind the distinct rheological properties of PCL100, PCL80LL20, and PCL80DL20, the crystallinity and hydrogen bonding of the samples were evaluated by XRD and ATR-FTIR. The XRD profile of the PU films is displayed in Fig. 4. The results indicated that the PCL100 was amorphous, and at a molar ratio of 20% of PLLA or PDLLA diol the PU became crystalline. Both the PLLA and PDLLA segment induced the crystallinity of the PCL segment, as evident by the PCL crystalline peaks at 2θ = 21.2° and 23.5°. For PCL80LL20, the PLLA crystalline peak at 2θ = 16.5° also appeared. Even though the PDLLA did not crystallize, the ability to induce PCL crystallization was greater than that of PLLA. The total amount of crystallinity in PCL80LL20 and PCL80DL20 was 12.48% and 17.66%, respectively. The crystallinity suggested the ability of the dispersion to self-assemble at higher temperatures.[16]

The ATR-FTIR spectra of PU films are shown in the ESI† (Fig. S3). The broad and weak absorbance peak at 3350 cm^{-1} was assigned to the –NH group in the hard segment. The continuous peak at 1730 cm^{-1} and 1670 cm^{-1} was attributed to the free carbonyl group and the hydrogen bound carbonyl group in the structure. The proportion of the bound to total C═O is listed in the ESI† (Table S3). After immersion in the culture medium, both the PCL80LL20 and PCL80DL20 increased while the PCL100 decreased in the extent of hydrogen bonding. This may explain the increased modulus of PCL80LL20 and

Published on 19 September 2016. Downloaded by Synchrotron Radiation Library on 11/09/2017 07:25:19.

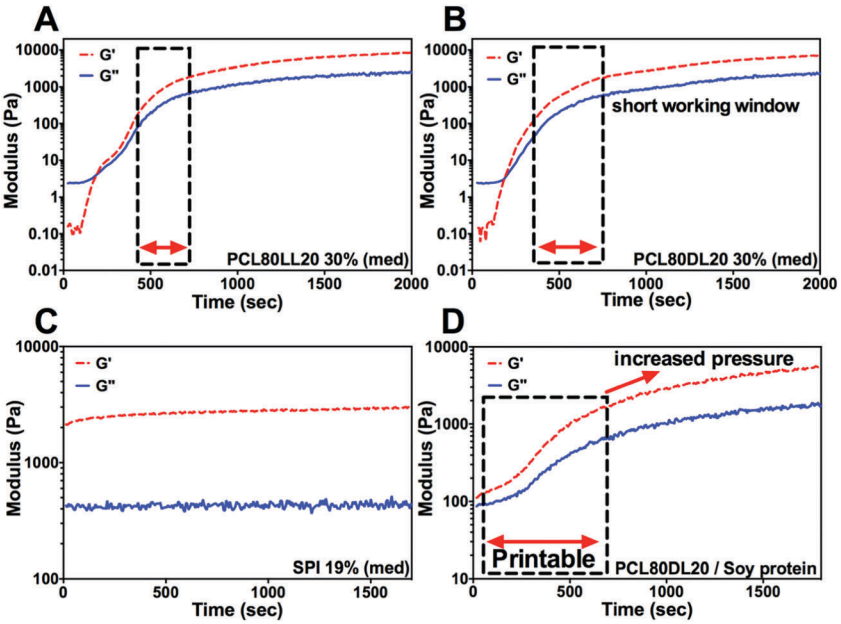

Fig. 3 Rheological properties of various dispersions (in medium) at 37 °C. The square box in each panel shows the approximate working window (time frame) for 3D printing. (A) PCL80LL20 30%, (B) PCL80DL20 30%, (C) soy protein isolate (19%), and (D) PCL80DL20 30% : SPI = 1 : 1.3 (the content of SPI 19%).

Table 4 Rheological properties of aqueous PU–SPI mixtures at 37 °C. (The PU employed was PCL80DL20 and in 30% of the final aqueous mixture.)

			Gel strength (G', Pa) at time					
Mix gels	Mix ratio	Gelation time (s)	1 min	5 min	10 min	20 min	30 min	tan δ (10 min)
SPI	—	NA	3360					0.18
SPI (med)	—	NA	3014					0.17
PU/SPI	1/1	NA	154	219	340	1372	2771	0.59
PU/SPI	1.2/1	NA	187	249	412	2348	4667	0.40
PU/SPI	1.3/1	NA	334	400	678	2847	4660	0.30
PU/SPI	1.4/1	NA	150	202	297	1386	2960	0.36
PU/SPI	1.5/1	143	9.04	37	360	2827	6960	0.35
PU/SPI	1.7/1	241	6.52	19.3	475	4066	7012	0.32
PU/SPI (med)	1.3/1	NA	130	338	1450	3532	5450	0.4

PCL80DL20 in the culture medium. The amount of calcium adsorption on the PU films is listed in the ESI† (Table S4). The results showed that the PCL100 surface adsorbed 2.5-times more calcium than the PCL80LL20 or PCL80DL20 surface.

3.7. 3D bioprinting of the cell-laden PU hydrogel and mixed gel

The PU/SPI hybrid gel as a bioink could be continuously printed with a dimension of 20 mm × 20 mm and thickness of 10 mm (Fig. 5A). Cells embedded in the hybrid hydrogel could survive and grow in 48 h. Fig. 5B shows the fibroblast morphology in the 3D printed structure of the hybrid gel, and Fig. 5C displays the NSC morphology in the hybrid gel. NSCs in the hybrid hydrogel revealed a round shape instead of a spindle shape.

3.8. Cell viability, proliferation, and metabolism

The viability of the NSCs in distinct hydrogels was evaluated immediately upon mixing using fluorescence imaging to characterize the cell health condition by counting the live/healthy, live/unhealthy, and dead cells (Fig. 6A). The results indicated that in the culture medium (control) about 81% of the NSCs were healthy and 17.3% of the NSCs were dead. In the PCL80LL20 hydrogel, 31% of the cells were alive and healthy, and 68.1% of the cells were dead. In the PCL80DL20 hydrogel, NSCs survived better with 52.4% live/healthy cells and 47% dead cells. These data indicated that the viability of the NSCs was reduced immediately when they were mixed with the hydrogel. Moreover, PCL80DL20 provided a better microenvironment for the survival of the embedded NSCs.

The images of the Ki-67 staining, which represented the proliferating NSCs in the hydrogels at 48 h, are depicted in Fig. 6B. On the basis of the fluorescent images, cells proliferated in both the PCL80DL20 and PCL80DL20/SPI hydrogels. The OCR values, an index of mitochondrial respiration, are shown in Fig. 6C. The OCR value of the NSCs was significantly reduced after culture in the PCL80LL20 and PCL80DL20 hydrogels. In particular, the NSCs in the PCL80DL20 hydrogel showed a

 This journal is © The Royal Society of Chemistry 2016

Published on 19 September 2016. Downloaded by Synchrotron Radiation Library on 11/09/2017 07:25:19.

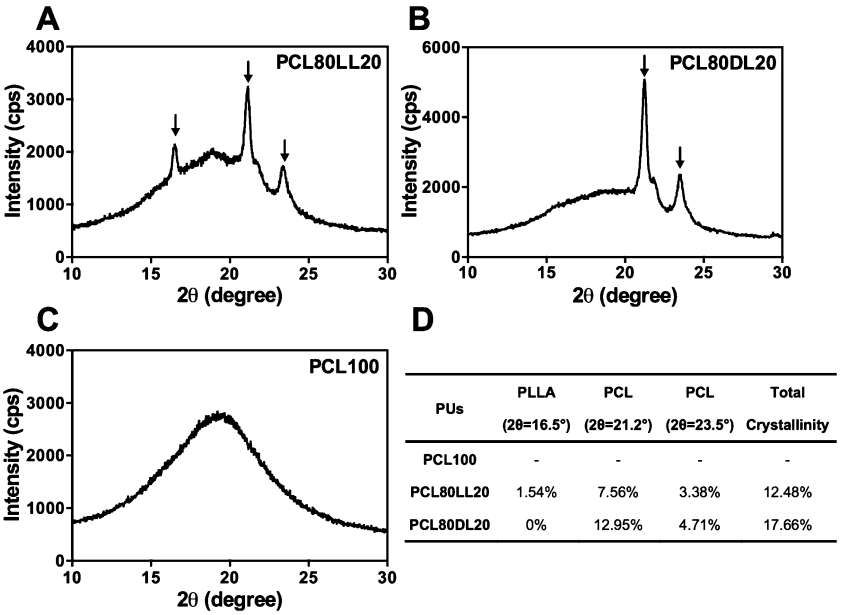

PUs	PLLA (2θ=16.5°)	PCL (2θ=21.2°)	PCL (2θ=23.5°)	Total Crystallinity
PCL100	-	-	-	-
PCL80LL20	1.54%	7.56%	3.38%	12.48%
PCL80DL20	0%	12.95%	4.71%	17.66%

Fig. 4 XRD profiles of various PUs in the solid state. (A) PCL80LL20, (B) PCL80DL20, (C) PCL100, and (D) the amount of crystallinity in PLLA, PDLLA, and PCL segments, respectively, as well as the total percentage of crystallinity in PU.

higher OCR value (~40.0 pmol min^{-1}) than those in the PCL80LL20 (~32.5 pmol min^{-1}). The PCL80DL20/SPI hydrogel rescued some mitochondrial respiration function of NSCs with an OCR value of 78.7 pmol min^{-1}.

The cell viability evaluated by the MTT assay at 48 h is given in Fig. S5 (ESI†). Cells in the PCL80LL20 gel had poor cell viability which decreased to 35% after 48 h of culture. Although the cell viability in the PCL80DL20 gel fell to 78% at 24 h, it increased to 124% after 48 h. The PCL80DL20/SPI hybrid gel had the best cell survival and growth. In the hybrid gel, the cell viability was maintained at 24 h and increased to 150% after 48 h of culture. However, 3D bioprinting manufacturing might injure cells because of extrusion and they may recover afterwards. The cell viability data obtained by the MTT assay may be overestimated.

3.9. Analysis of gene expression for NSCs in hydrogels

The gene expression, including nestin, β-tubulin, MAP2, and GFAP, for NSCs in hydrogels or those on the tissue culture polystyrene plates (TCPS) at 3 days is presented in Fig. 7. The expression level of nestin significantly increased for NSCs embedded in the PCL80DL20 and PU/SPI hybrid hydrogels compared to those in the TCPS control. The expression of nestin for NSCs in the PU/SPI hybrid hydrogel was also higher than that in the PCL80DL20 (~3.7-fold). NSCs encapsulated in the PU-based hydrogels expressed more MAP2 (mature neuronal marker) and GFAP (glial marker) genes than those in TCPS. Moreover, the gene expression levels of MAP2 and GFAP were enhanced by about 5.0-fold and 6.8-fold, respectively, when NSCs were embedded in the PU/SPI hybrid hydrogel compared to those in the pure PCL80DL20 hydrogel. Meanwhile, the NSCs embedded in the PCL80DL20 hydrogel had the greatest β-tubulin (early neuronal marker) gene expression and those in the PU/SPI hybrid gel had the lowest. The MAP2 gene expression profiles revealed that both the PCL80DL20 pure hydrogel and hybrid hydrogel had a tendency to promote the neuronal differentiation of NSCs. Some NSCs in the PCL80DL20/SPI hybrid gel may differentiate into glial cells.

4. Discussion

Three waterborne PU nanoparticle dispersions composed of different ratios of oligodiols in the soft segment were synthesized and characterized in this study. PU nanoparticles were stably dispersed in water at 25 °C because of the negative charge of the dissociated hydrophilic group (–COOH).

The nanoparticle size is one of the essential parameters to determine the physico-chemical properties. The R_h of the nanoparticles was obtained on the basis of Brownian motion, where the diffusion velocity and the mobility were highly affected by the environmental temperature. When the temperature of the dispersion was raised from 25 °C to 37 °C, PCL100 had no R_h change while PCL80LL20 and PCL80DL20 showed slight increases in R_h. However, the SAXS measurement at 25 °C and 37 °C revealed that the average size of PCL80LL20 increased dramatically at 37 °C, while that of PCL80DL20 was the same at both temperatures. The mobility and the free volume of the molecular chain in a nanoparticle may account for the temperature-dependent properties. As the soft segment of the PU contained PLA (PLLA or PDLLA) and PCL segments, the thermodynamic incompatibility between PCL and PLA segments could contribute to microphase separation.[20] This may produce additional free volume in the nanoparticles. The molecular chains in the PU nanoparticles may become more mobile at higher temperatures, and in water, the nanoparticles may swell.[20] The PDLLA segment did not form ordered

Published on 19 September 2016. Downloaded by Synchrotron Radiation Library on 11/09/2017 07:25:19.

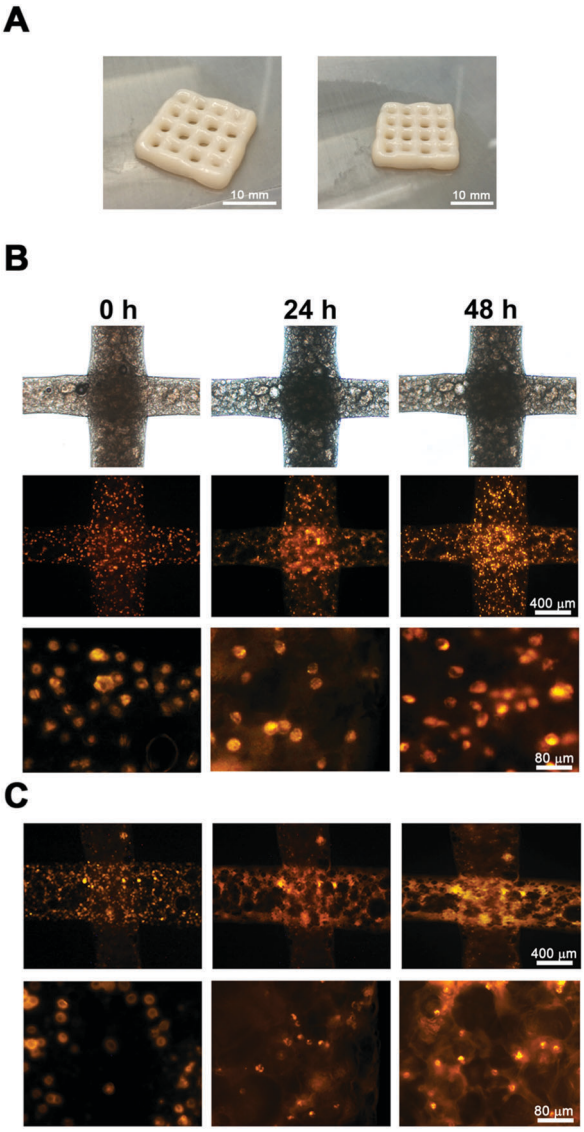

Fig. 5 Cell printing with various hydrogels. (A) The gross appearance of 3D bioprinted scaffolds of the PCL80DL20/SPI hybrid hydrogel. (B) Red fluorescence (PKH26)-labelled fibroblasts in the PCL80DL20/SPI hybrid hydrogel scaffolds at various time points (0, 24, and 48 h). (C) PKH26-labeled neural stem cells (NSCs) in the PCL80DL20/SPI hybrid hydrogel scaffolds at 0, 24, and 48 h.

structures in PU as easily as PLLA because of steric hindrance, and thus PCL80DL20 may have more free volume and less temperature-responsive size changes than PCL80LL20. As the temperature further increased to 60 °C (a temperature higher than the softening temperature of the PCL and PLA segments), both the PCL80LL20 and PCL80DL20 nanoparticles increased their sizes *vs.* 25 °C, indicating that the PCL and PLA segments were both mobile at this time. In particular, the size increase of PCL80DL20 at 60 °C was more obvious than that of PCL80LL20, suggesting the capacity of PCL80DL20 to swell and form a packing structure once the situation allows.

In the cell culture media or electrolyte-containing media, an osmotic pressure difference may cause PU nanoparticles to shrink. The nanoparticles of PCL80DL20, with a presumably greater free volume, shrank more significantly than those of PCL80LL20. The less negative zeta potential of the nanoparticles in the presence of electrolytes implied the hydrodynamic screening on the particle surface.[28] The high electrolyte concentration further produced a salting out effect, leading to particle aggregation.[29] According to the profiles, the PU nanoparticles of either PCL80LL20 or PCL80DL20 in the culture medium had short inter-particle distances and formed fractal network structures with a fractal dimension D_f around 2.8 to 3.2. According to recent literature, the fractal structure of a hydrogel can influence cell proliferation and fate.[30]

The shortened distance among the PU nanoparticles may enhance the secondary force interaction (*e.g.*, hydrogen bond) to undergo a sol–gel transition at higher temperatures.[20] The factors that influence the sol–gel transition and gel modulus include the probability for particle collisions (*i.e.*, solid contents) and the interaction between adjacent particles (*e.g.*, the degree of packing). The PU with 25% and 30% solid content in water was above the critical concentration for interaction, and the sol–gel transition could occur at 37 °C. Meanwhile, 30% compared to 25% solid content gave a shorter gelation time and higher gel modulus at 37 °C, in particular for the more thermo-responsive PCL80LL20 nanoparticles. In electrolytes or culture media, the hydrodynamic screening effect promoted gelation and increased the gel modulus, in particular for the more salt-sensitive PCL80DL20 nanoparticles. Besides, the hydrophobic interaction serving as the driving force for amphiphile aggregation is commonly entropy-driven and electrolyte-dependent.[31] Hydrophobic associations plus the electrolyte screening helped the PCL80DL20 gel reach a significantly greater modulus, especially 5 min after the transition ($\sim$10–100 times *vs.* in water). When the gelation and packing tried to achieve a final balanced structure at 30 min, both PCL80LL20 and PCL80DL20 gels showed stronger a gel modulus (*vs.* in water) because of the close packing network ($D_f > 2.5$). At this time (30 min), the gels in the culture media had a dynamic modulus of 6–8 kPa and a tan δ value of 0.28–0.34, which are reasonable values for further applications.

To clarify the distinct rheological properties among the various PU dispersions, the crystallinity, hydrogen bonding, and calcium adsorption of the PUs were further examined. The XRD profile showed the amorphous PCL segment in the sample of PCL100, while the profile of PCL80LL20 demonstrated PLLA as well as PCL crystalline peaks, which was consistent with our previous findings.[20] Surprisingly, the amorphous PDLLA in the PCL80DL20 caused an even higher portion of PCL segments to crystallize in the current study. We hypothesized that the thermodynamic incompatibility between the PCL and PDLLA segments and the amorphous nature of PDLLA may force the PCL segment to align and become ordered. This hypothesis also agreed with the presumed greater free volume of the PCL80DL20. On the other hand, the altered secondary force on the PU in the presence of the culture medium may affect the thermo-responsive properties. The surface of the PCL-based waterborne PU could undergo functional group rearrangement in the culture medium because of the flip-out of the hydrophilic

 This journal is © The Royal Society of Chemistry 2016

Published on 19 September 2016. Downloaded by Synchrotron Radiation Library on 11/09/2017 07:25:19.

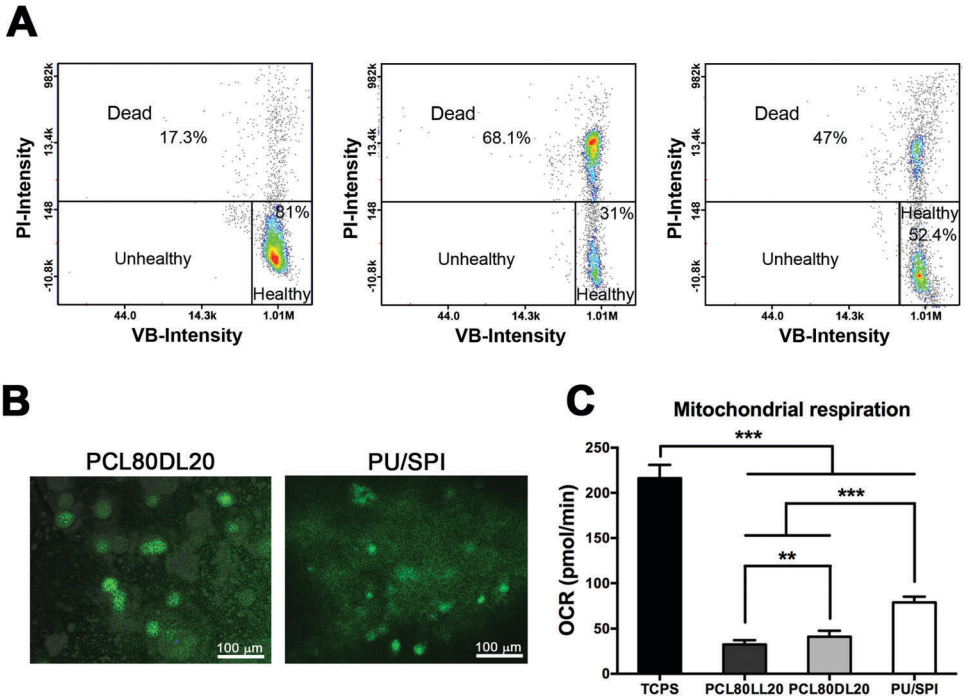

Fig. 6 Survival and proliferation of NSCs in various hydrogels. (A) The survival of NSCs immediately after embedding in various hydrogels determined by fluorescence imaging. (B) Immunohistochemical staining of the Ki67 protein shows the proliferating cells at 48 h. (C) The mitochondrial respiration of NSCs in various hydrogels after 24 h culture.

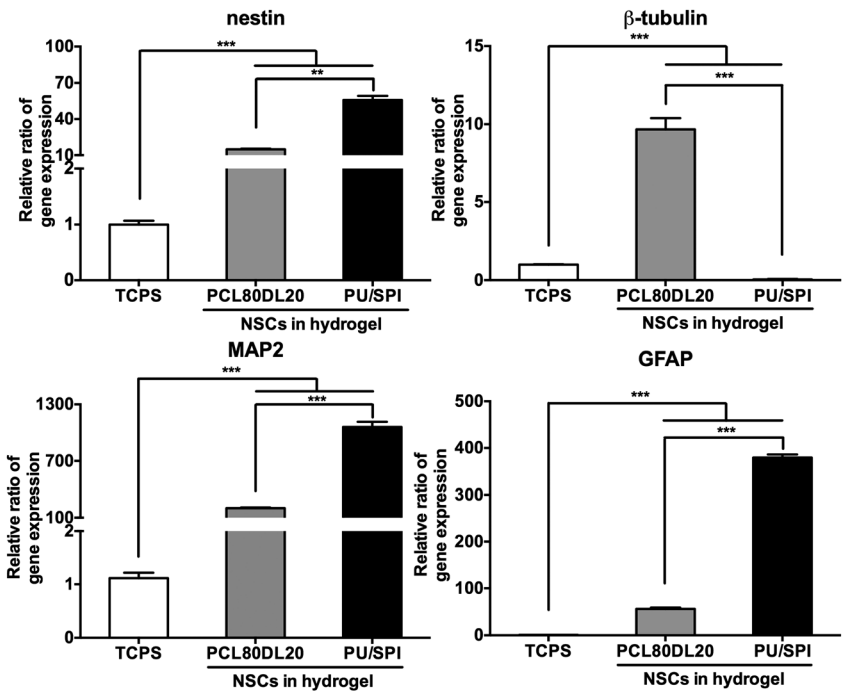

Fig. 7 The expression of specific neuronal-related genes (nestin, β-tubulin, MAP2, and GFAP) for the printed NSCs analyzed by real-time RT-PCR at 72 h. The gene expression was represented as the relative ratio to the group of tissue culture polystyrene (TCPS). *$p < 0.05$ was considered statistically significant.

group (–COO^-, –NH) in the aqueous media that was further stabilized by the calcium cage.[32] The ATR-IR results in this study indicated a more bonded carbonyl group on PCL80LL20 and PCL80DL20 after immersion in the culture medium, and the opposite was true for PCL100. Moreover, the PCL100 cast films adsorbed more calcium, which appeared to compete with

Published on 19 September 2016. Downloaded by Synchrotron Radiation Library on 11/09/2017 07:25:19.

the hydrogen bonding. The strong cage effect of PCL100 in the culture medium with calcium and hydrophilic groups (–COO^-, –NH) may screen the hydrogen bonding and other secondary forces in the original water dispersion, resulting in a lack of thermo-responsive properties in PCL100.

Although PCL80DL20 (in culture medium at 37 °C) achieved a greater storage modulus value in the initial 5 min (53.3 Pa) compared to that of PCL80LL20 (15.7 Pa), the rheological properties of the hydrogel were still not enough for continuous 3D layer-by-layer deposition. In order to shorten the gelation time and expand the working window for multi-layer cell printing, SPI was blended with the PU dispersion. Extracted from soybeans, SPI has been widely applied in food industries and biotechnology because of its good biodegradability and processability.[33–35] The combination of SPI with other materials could offer a physical or chemical interaction, which may enhance the gel properties and biocompatibility.[36,37] In the literature, the PU/SPI blended thermoplastic film exhibited fine compatibility, flexibility, and a lower cytotoxicity than PU.[38] Based on the rheological studies on different blending ratios of SPI and PU, SPI did increase the initial viscosity for printing, and the hybrid gel cured more quickly for 3D deposition. In our study, the modulus of the optimized hybrid gel (PU : SPI = 1.3 : 1) was improved to 338 Pa in 5 min with a small tan δ value (0.31), indicating the elastic-like properties of the gel for immediate printing and deposition. To sum up, the gelation time and the storage modulus after gelation are the two prominent rheological factors for the selection of a suitable composite hydrogel for 3D bioprinting. During the optimization process, the concentration of the SPI additive in the hybrid hydrogel and the solid content of the PU dispersion as well as the effect of the ions were all considered. In this study, PU with a solid content of 30% possessed a higher gelation ability and the culture medium containing calcium ions could further modify the network structure to result in particle aggregation in the PCL80DL20 hydrogel. Although SPI was dissolved in PBS, the effect of the ions was reduced upon mixing. Therefore, we assumed that it was SPI instead of the increased number of ions that affected the rheology of the final gel. PU had a fractal dimension close to 3, and SPI was previously reported to have a fractal dimension of 1.2.[24] The hybrid gel did not show a fractal structure based on the SAXS profile (Fig. S4, ESI†). This was probably because of the heterogeneous network structure of the hybrid. Investigation on the exact interaction between SPI and PU is still required to identify the mechanism for the unique viscoelasticity of the hybrid PU/SPI system.

To evaluate the tissue engineering applications of our synthesized bioink, neural stem cells (NSCs) were embedded in the hydrogels and analyzed for cell viability, metabolism, proliferation, and gene expression of neural-related markers. The data suggested potential for tissue engineering applications, particularly in the field of neural repair. Results indicated that some cells were not healthy in the initial condition. However, the healthy cells (~52%) may start to grow in 2 days. An earlier study on repairing an adult zebrafish brain injury also confirmed better cell viability in PCL80DL20 *vs.* PCL80LL20.[21] Cell death and a poor health condition might be a result of hydrogel mixing and shear rate during extrusion.[39] The images of Ki-67 immunostaining for cells at 48 h confirmed the proliferation of NSCs in the PCL80DL20 and PCL80DL20/SPI hydrogels. Moreover, the hybrid of PU and SPI provides a good working window for 3D printing and deposition and improves the cytocompatibility. When comparing the oxygen consumption rate of NSCs in the pure PU hydrogel and PU/SPI hybrid gel after culture, the NSCs in the PU/SPI had a higher OCR value, indicating that SPI may provide a better 3D environment for NSCs. The embedded NSCs had limited extension in the 3D bioprinted constructs. Although the radial or horizontal orientation of NSCs was not discovered, NSCs in 3D constructs demonstrated a differentiation tendency toward neuronal and glial cells according to the further examination of the gene expression. By tuning the stiffness of the hydrogels, it may be possible to further modulate cell morphology in the future. NSCs in hydrogels are characterized by high levels of nestin expression. Cells that differentiate into neurons and glia can be identified by the increased expression of MAP2, β-tubulin, and GFAP. MAP2 is a neuron-specific cytoskeletal protein that is used as a marker of mature neuronal phenotype, while the expression of neuron-specific β-tubulin is expressed during the early development. NSCs in the PCL80DL20/SPI hydrogel expressed the lowest level of β-tubulin gene and higher grades of MAP2 and GFAP compared to those of pure PCL80DL20 at 3 d of culture, indicating that the NSCs embedded in the PCL80DL20/SPI hydrogel had further differentiated during the culture period. Based on the above observation, SPI may offer a proper niche for NSC differentiation into mature neurons as well as promote some NSCs to differentiate into glial cells. The unique structure-dependent gelation mechanism of various thermo-responsive PUs and the tunable rheological properties of PUs with the other biological gels may allow the establishment of a range of PU bioink formulae for applications in 3D bioprinting and neural tissue engineering or other tissue engineering applications in the future.

5. Conclusions

A hybrid thermo-responsive 3D bioprinting ink composed of PU dispersions and SPI was developed. The thermo-responsive properties and rheological behavior of PU were attributed to interparticle interactions, which were affected by the electrolyte as well as the cell culture media. The SAXS measurements revealed a fractal structure with a fractal dimension in the range of 2–3 for PU dispersions after thermal gelation. Replacing the soft segment of the PCL-based PU with 20 mol% of the amorphous PDLLA segment strongly induced the crystallization of the PCL segment. The above PU (PCL80DL20) was also salt-sensitive, could gel faster at 37 °C and possessed the potential as thermo-responsive hydrogel for 3D printing. In particular, PCL80DL20 blended with SPI created a good storage modulus (G') working window during 3D deposition and demonstrated excellent cytocompatibility for direct cell printing. Moreover, the PU/SPI hybrid gel provided a better microenvironment for

 This journal is © The Royal Society of Chemistry 2016

Published on 19 September 2016. Downloaded by Synchrotron Radiation Library on 11/09/2017 07:25:19.

the survival, proliferation, and metabolism of neural stem cells and their differentiation into neural cells. The PU hybrid with SPI may have potential to create a unique group of inks for 3D bioprinting in neural tissue engineering.

Acknowledgements

This work was supported by the Program for Additive Manufacturing (MOST104-2218-E-002-010), Ministry of Science and Technology, the University Cutting-Edge Steering Research Project (NTU-CESRP-103R104943), Ministry of Education, and National Health Research Institutes (CS-105-SP-02), Taiwan, ROC. We are also grateful to Dr U-Ser Jeng in National Synchrotron Radiation Research Center for the technical assistance.

References

1 Alzheimer's Association, *Alzheimer's Dementia*, 2015, **11**, 332.
2 R. Y. Tam, T. Fuehrmann, N. Mitrousis and M. S. Shoichet, *Neuropsychopharmacology*, 2014, **39**, 169–188.
3 D. De Feo, A. Merlini, C. Laterza and G. Martino, *Curr. Opin. Neurol.*, 2012, **25**, 322–333.
4 T. Matsui, W. Akamatsu, M. Nakamura and H. Okano, *Exp. Neurol.*, 2014, **260**, 12–18.
5 K. Young, T. Walker and J. Huang, *Stem Cells Int.*, 2016, **2016**, DOI: 10.1155/2016/1890568.
6 H. Kim, M. J. Cooke and M. S. Shoichet, *Trends Biotechnol.*, 2012, **30**, 55–63.
7 Q. Gu, E. Tomaskovic-Crook, R. Lozano, Y. Chen, R. M. Kapsa, Q. Zhou, G. G. Wallace and J. M. Crook, *Adv. Healthcare Mater.*, 2016, DOI: 10.1002/adhm.201600095.
8 S.-J. Lee, W. Zhu, N. Castro and L. G. Zhang, *J. Neural Eng.*, 2016, 1–24.
9 I. T. Ozbolat and M. Hospodiuk, *Biomaterials*, 2016, **76**, 321–343.
10 B. Duan, L. A. Hockaday, K. H. Kang and J. T. Butcher, *J. Biomed. Mater. Res., Part A*, 2013, **101**, 1255–1264.
11 J. Jia, D. J. Richards, S. Pollard, Y. Tan, J. Rodriguez, R. P. Visconti, T. C. Trusk, M. J. Yost, H. Yao and R. R. Markwald, *Acta Biomater.*, 2014, **10**, 4323–4331.
12 C. Norotte, F. S. Marga, L. E. Niklason and G. Forgacs, *Biomaterials*, 2009, **30**, 5910–5917.
13 X. Wang, Y. Yan, Y. Pan, Z. Xiong, H. Liu, J. Cheng, F. Liu, F. Lin, R. Wu, R. Zhang and Q. Lu, *Tissue Eng.*, 2006, **12**, 83–90.
14 A. Skardal, J. Zhang, L. McCoard, X. Xu, S. Oottamasathien and G. D. Prestwich, *Tissue Eng., Part A*, 2010, **16**, 2675–2685.
15 T. Billiet, E. Gevaert, T. De Schryver, M. Cornelissen and P. Dubruel, *Biomaterials*, 2014, **35**, 49–62.
16 K. Kobayashi, C.-i. Huang and T. P. Lodge, *Macromolecules*, 1999, **32**, 7070–7077.
17 S. Grad, L. Kupcsik, K. Gorna, S. Gogolewski and M. Alini, *Biomaterials*, 2003, **24**, 5163–5171.
18 P. A. Gunatillake and R. Adhikari, *Eur. Cells Mater.*, 2003, **5**, 1–16.
19 J. D. Fromstein and K. A. Woodhouse, *J. Biomater. Sci., Polym. Ed.*, 2002, **13**, 391–406.
20 C.-W. Ou, C.-H. Su, U.-S. Jeng and S.-h. Hsu, *ACS Appl. Mater. Interfaces*, 2014, **6**, 5685-5694.
21 F.-Y. Hsieh, H.-H. Lin and S.-h. Hsu, *Biomaterials*, 2015, **71**, 48–57.
22 K. B. Chien and R. N. Shah, *Acta Biomater.*, 2012, **8**, 694–703.
23 G. Silva, C. M. Vaz, O. Coutinho, A. Cunha and R. Reis, *J. Mater. Sci.: Mater. Med.*, 2003, **14**, 1055–1066.
24 A. Merolli, L. Nicolais, L. Ambrosio and M. Santin, *Biomed. Mater.*, 2010, **5**, 015008.
25 K. B. Chien, E. Makridakis and R. N. Shah, *Tissue Eng., Part C*, 2012, **19**, 417–426.
26 S.-h. Hsu, K.-C. Hung, Y.-Y. Lin, C.-H. Su, H.-Y. Yeh, U.-S. Jeng, C.-Y. Lu, S. A. Dai, W.-E. Fu and J.-C. Lin, *J. Mater. Chem. B*, 2014, **2**, 5083–5092.
27 S. R. Kline, *J. Appl. Crystallogr.*, 2006, **39**, 895–900.
28 D. O. Riese, G. H. Wegdam, W. L. Vos, R. Sprik, D. Fenistein, J. H. Bongaerts and G. Grübel, *Phys. Rev. Lett.*, 2000, **85**, 5460.
29 H. Dautzenberg, *Macromolecules*, 1997, **30**, 7810–7815.
30 K.-C. Hung, U.-S. Jeng and S.-h. Hsu, *ACS Macro Lett.*, 2015, **4**, 1056–1061.
31 H. Christenson, P. Claesson, J. Berg and P. Herder, *J. Phys. Chem.*, 1989, **93**, 1472–1478.
32 K. C. Hung and S. h. Hsu, *Adv. Healthcare Mater.*, 2015, **4**, 2186–2194.
33 R. Kumar, D. Liu and L. Zhang, *J. Biobased Mater. Bioenergy*, 2008, **2**, 1–24.
34 C. M. Vaz, J. Mano, M. Fossen, R. Van Tuil, L. De Graaf, R. Reis and A. Cunha, *J. Macromol. Sci., Part B: Phys.*, 2002, **41**, 33–46.
35 H. Xu, S. Cai, A. Sellers and Y. Yang, *RSC Adv.*, 2014, **4**, 15451–15457.
36 J. M. Renkema, H. Gruppen and T. Van Vliet, *J. Agric. Food Chem.*, 2002, **50**, 6064–6071.
37 S. Silva, M. Santos, O. Coutinho, J. Mano and R. Reis, *J. Mater. Sci.: Mater. Med.*, 2005, **16**, 575–579.
38 H. Tian, Y. Wang, L. Zhang, C. Quan and X. Zhang, *Ind. Crops Prod.*, 2010, **32**, 13–20.
39 Y. Yu, Y. Zhang, J. A. Martin and I. T. Ozbolat, *J. Biomech. Eng.*, 2013, **135**, 091011.